Recoil energy dependence of primary radiation damage in tungsten from cascade overlap with voids

Fellman, A.

2022-12-15

Fellman , A & Sand , A E 2022 , ' Recoil energy dependence of primary radiation damage in tungsten from cascade overlap with voids ' , Journal of Nuclear Materials , vol. 572 , 154020 . https://doi.org/10.1016/j.jnucmat.2022.154020

http://hdl.handle.net/10138/351964
https://doi.org/10.1016/j.jnucmat.2022.154020

Journal of Nuclear Materials 572 (2022) 154020

Contents lists available at ScienceDirect

Journal of Nuclear Materials

journal homepage: www.elsevier.com/locate/jnucmat

Recoil energy dependence of primary radiation damage in tungsten from cascade overlap with voids

A. Fellman[a], A.E. Sand[a,b,*]

[a] Department of Physics, University of Helsinki, P.O. Box 43, FI-00014, Finland
[b] Department of Applied Physics, Aalto University, Aalto FI-00076, Finland

ARTICLE INFO

Article history:
Received 10 May 2022
Revised 4 September 2022
Accepted 5 September 2022
Available online 7 September 2022

Keywords:
Tungsten
Molecular dynamics
Cascade overlap
Radiation damage
Dislocations

ABSTRACT

Models of radiation damage accumulation often assume a constant rate of additional primary damage formation during prolonged irradiation. However, molecular dynamics simulations have shown that the presence of pre-existing radiation-induced defects modifies the numbers of additional defects formed from individual cascades. In this work, we study the formation of defects in tungsten for a range of primary recoil energies, for cascades that fully overlap with pre-existing voids of different sizes. We extend a recent model describing defect production in the presence of pre-existing damage to also account for the recoil energy dependence, and parametrize the extension based on our simulation data. We also analyze the morphology of the primary damage from cascades overlapping with voids, and show that the in-cascade formation of ⟨100⟩ dislocation loops in such events is more dependent on the size of the pre-existing void, than on the energy of the primary recoil.

1. Introduction

In environments where materials are subjected to large radiation doses, critical components should have favourable properties in regard to resisting radiation damage. Tungsten (W) has been identified as a promising candidate for plasma facing components in future fusion reactors, in particular as a divertor material [1–4]. Understanding the accumulation of radiation damage in tungsten is thus of great interest in order to understand the changes to the mechanical properties that the material in these components will undergo during their operational lifetimes.

Significant effort has been invested into the modelling of tungsten in fusion reactor conditions [5]. The formation of primary radiation damage in pristine tungsten crystal has been studied extensively using molecular dynamics (MD) simulation methods [6]. However, in applications where materials are subjected to high doses of radiation, overlap between collision cascades and previously accumulated damage becomes probable. The effects of cascade-defect overlap changes the damage formation characteristics of the cascade.

Experimentally, it has been shown that the defect density in iron increases non-linearly with radiation dose [7]. This was later demonstrated using computer simulations of cascade overlap, where the number of new defects was reduced as a consequence of overlap [8]. Since then, simulations of cascade overlap have been carried out in a number of materials, including Ni and Ni-based alloys [9], Fe and Fe-based alloys [10–12], equiatomic multicomponent alloys [13,14], Zr [15–17] and recently also in $In_xGa_{1-x}N$ [18].

Cascades are highly stochastic events, with a wide variety of outcomes, and one challenge with obtaining sufficient statistics to draw quantitative conclusions from simulations of cascades overlapping with previous cascades is that both the initial and subsequent cascade damage will vary strongly. With the significant increase in computer power seen in the last decade, more and more studies have been carried out with up to a thousand or more overlapping cascades [10,13,14,19,20]. Although such work has given insights into damage accumulation at higher radiation dose, the limited time scale that can be reached by molecular dynamics simulations restricts the consideration of diffusion processes occurring between cascades. Thus, the results of such studies essentially pertain to an a-thermal limit.

This issue can be addressed by approaching the question from a different perspective, by considering ideal defects as the underlying damage, rather than the defects produced directly in prior cascade simulations. Such studies assume the relaxed, thermally evolved defect as the initial state of the system. The effects of cascades have been studied in the presence of pre-existing point

* Corresponding author at: Department of Applied Physics, Aalto University, Aalto FI-00076, Finland.
E-mail address: andrea.sand@aalto.fi (A.E. Sand).

https://doi.org/10.1016/j.jnucmat.2022.154020

defects in several materials [21], and overlapping with dislocation loops in Fe and FeCr [22] and in W [23].

Another restriction on the study of multiple overlapping cascades is in regards to the cascade energy that has been considered. Higher energy cascades require larger simulation cells, but also significantly smaller integration time steps during the initial energetic cascade development, resulting in a much more than $\mathcal{O}(n)$ increase in the total computational cost of each cascade simulation, and prohibitively increasing the cost of series of multiple such simulations. In tungsten, however, energetic recoils produce qualitatively different damage than that produced by less energetic recoils [24,25], and energetic recoils occur with considerable frequency under a fusion neutron spectrum [26]. Recent investigations of energetic cascades overlapping with pre-existing damage in tungsten have shown that overlap with prior cascade damage causes pronounced changes to the morphology of the defects produced [27].

A characteristic property of accumulating damage in overlapping cascade simulations with MD is that large vacancy clusters and voids do not form, due to the lack of time for diffusion processes to be active during the simulations. However, nanometer-sized voids form readily under neutron irradiation [28]. Cascades have the effect of recombining defects in the material volume encompassed by the cascade [21,27], hence there is a competition between cascade-induced recombination and void formation, which cannot be modelled directly with simulations of cascades overlapping prior cascade damage. Previously, we have simulated cascade overlap in tungsten with pre-existing vacancy type defects [29], and found morphology changes such as $1/2\langle 1\,1\,1\rangle$ dislocation loops changing to $\langle 1\,0\,0\rangle$ as a result of the overlapping cascade. Additionally, $\langle 1\,0\,0\rangle$ vacancy-type dislocation loops were found to form in cases of partial overlap with voids.

In [23], a model was introduced that describes the number of new defects produced by 10 keV cascades in Fe and W, as a function of the degree of overlap between the cascade and interstitial defects. The model also applies well to the case of vacancy type defects in W, including both voids and dislocation loops [29]. Here, we extend this previous work, and investigate the impact of the initial cascade energy on the formation of new defects from cascades overlapping with pre-existing voids in W, for cascade energies up to 100 keV. The original model is extended to include the primary knock-on atom (PKA) energy as a parameter, and fitted to an extensive data set generated from cascade simulations at different energies, overlapping with voids of different sizes. The article is structured as follows: In Section 2, we describe the original model, and Section 3 gives the details of the simulation methods and the analysis techniques used in the current work. In Section 4, our simulation results are presented and the model extension is described and parametrized. Finally, in Section 5 we discuss the implications of our results, and the range of validity of the model. Section 6 concludes the work.

2. Model for overlapping cascade damage

In previous work [23,29], an analytical model was introduced to describe the number of new defects produced as a function of the degree of overlap between the cascade and a pre-existing defect. The model was created to capture the overlapping behaviour observed from MD simulations. A number of conditions can be identified that the model should uphold. Firstly, when the cascade and defect are not overlapping, the number of new defects should correspond to the value produced from a cascade in pristine material. Secondly, based on simulation results, the increased size of the pre-existing defect should decrease the number of new defects produced. Finally, the model should be able to capture the behaviour observed at full overlap. These considerations led to the following model [23]:

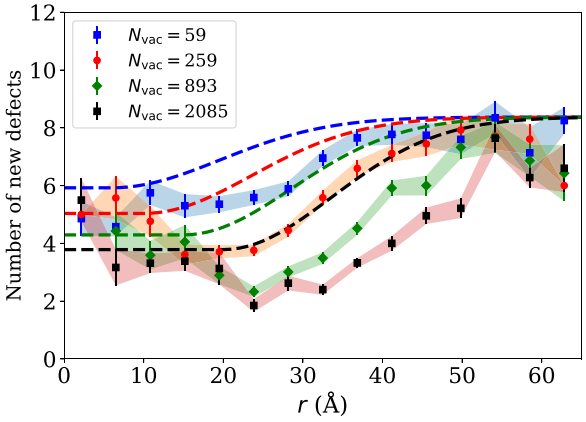

Fig. 1. Number of new Frenkel pairs created in 10 keV cascade simulations on pre-existing voids, as a function of the separation r between the cascade midpoint and the defect centre. Data taken from Ref. [29]. (N_{vac}: number of vacancies in the initial defect). The data is binned based on the separation distance r. Each point represents average values of each bin and the uncertainty is given as the standard error.

$$N = \begin{cases} N_{\text{new}}, & r < r_{\text{defect}} \\ N_0 - (N_0 - N_{\text{new}}) \exp\left[-\frac{(r - r_{\text{defect}})^2}{r_{\text{casc}}^2} \right], & r \geq r_{\text{defect}}, \end{cases} \tag{1}$$

where, r is the distance between the center of the defect and the center of the collision cascade, r_{casc} is the cascade radius, and r_{defect} is the radius of the initial defect. N_0 is the average number of defects formed from a cascade in a perfect material (this is potential dependent and determined from simulations), while N_{new} is defined as the number of new point defects during cascade overlap with the pre-existing vacancy-type defect. From Fellman et al. [29], N_{new} depends on the size of the pre-existing defect according to Eq. (2).

$$N_{\text{new}} = \begin{cases} N_0, & N_{\text{vac}} = 0 \\ N_0 - a \ln N_{\text{vac}}, & N_{\text{vac}} > 0 \end{cases} \tag{2}$$

Here, N_0 is again the number of new defects in pristine material and N_{vac} describes the size of the pre-existing defect in terms of the number of vacancies it contains. In previous work [29], the parameter a was fitted to data obtained from 10 keV cascade simulations. The aim of the current study is to describe the dependence of this parameter on the PKA energy.

Fig. 1 shows an example case of Eq. (1) fitted to simulation data from Fellman et al. [29], with different sizes of voids as the pre-existing defects, and a cascade energy of 10 keV. The numbers of new defects were determined in Fellman et al. [29] as a function of the distance between the cascade center and the pre-existing void. As seen in the figure, the behaviour at partial overlap is very similar to that of full overlap, with the number of new defects at full overlap giving an upper bound to the numbers of defects formed also at partial overlap. For larger voids in particular, in the region with partial overlap at a separation distance between 20 and 30 Å, there is a minimum in the defect numbers, which Eq. (1) does not capture. A similar decrease was not seen for cascade overlap with vacancy-type dislocation loops [29]. The model thus provides an upper bound on the additional defect count for cascades overlapping with voids. In the current study, we focus on the region of full and partial overlap between the cascade and the pre-existing void, and rely on the original model to describe the transition to the non-interacting regime, since obtaining statistics for high energy cascades over the whole range of separation distances would be computationally infeasible.

Table 1
The pre-existing void sizes used in this study, in terms of numbers of vacancies N_{Vac} and the corresponding void radius r_{void}.

N_{vac}	r_{void} (Å)
(27, 59, 259, 893, 2085)	(5, 6, 10, 15, 20)

3. Methods and analysis

Voids of different sizes were created by defining a radius from the middle of the simulation cell, and removing the atoms inside this region. Table 1 lists the void sizes in both numbers of vacancies and in terms of the corresponding radius of the void. Systems containing clusters with 10 or fewer vacancies were also created, by removing individual atoms from a roughly spherical region. These smaller vacancy clusters, since they are not perfectly spherical due to the discreteness of the lattice, were not defined by a radius, but rather by the number of atoms that were removed. Hence, in what follows, we do not report the radius of such defects.

The cells were then equilibrated at 300 K and 0 kbar, with the temperature and pressure scaled using a Berendsen thermostat and barostat [30]. The simulation cell size was chosen so that the whole cascade region could be contained within the cell. We used periodic boundary conditions in the cascade simulations, and if an atom crossed the border with over 10 eV kinetic energy, the simulation was aborted and a new simulation was performed. This way the self-interaction of the cascade over the borders was limited. During the simulation, a Berendsen thermostat set to 300 K was applied to the border atoms. The total simulation times were chosen such that the average temperature of the system decreased to within a few Kelvin of the initial temperature, at which point the collision cascade had fully recrystallized. All simulations were performed using the PARCAS molecular dynamics code [31].

The PKA atom was chosen by generating random directions evenly distributed over a sphere. An atom was then selected closest to the point at 15 Å from the center of the simulation cell in the chosen direction. This atom was then given a kinetic energy corresponding to the desired cascade energy, in the direction towards the center of the cell, which was also the center of the pre-existing void. Although higher energy PKAs will travel further, the likelihood for the cascade to develop at an angle to the initial PKA direction also increases with increasing PKA energy. Because of this, we chose to use the same displacement of 15 Å from the center for all PKA energies, so that all cascades overlapped either fully or partially with the void. For the largest voids, the cascade is thus initiated at the edge of the void, by a PKA initially traversing the void. In the analysis, we consider all simulated cascades.

We used the Finnis–Sinclair potential by Ackland et al. [32] (hereafter referred to as AT-ZN), which has been widely used for radiation damage simulations [24,33,34], including previous studies that we compare to in this work [23,29]. The potential was hardened for short range interactions by Zhong et al. [33], by smoothly joining to the Ziegler–Biersack–Littmark universal interatomic potential [35]. Properties such as the melting point and threshold displacement energy are accurately predicted by this potential, which also predicts the formation of central vacancy clusters from ion impacts in good agreement with field ion microscopy experiments [33]. Furthermore, the AT-ZN potential correctly predicts the formation energy of $1/2\langle 1\,1\,1\rangle$ type loops as lower than the formation energy of $\langle 1\,0\,0\rangle$ loops, for all loop sizes [23]. Hence, we conclude that the cascade annealing and recrystallization process is well described by this potential. We have also shown in a previous study [29], that the number of additional defects formed from 10 keV cascades overlapping with voids is similar for three different potentials, including the AT-ZN potential, when considered relative to the number of defects formed in the pristine crystal with the respective potentials. Here, in order to obtain sufficient statistics to draw quantitative conclusions from higher energy cascade simulations with different initial void sizes, we employ only one potential.

In Table 2, we list the numbers of simulations performed for each void size and PKA energy. Not all pre-existing void sizes were simulated for the higher energy cascades, due to the high computational cost of such simulations.

The resulting damage was analysed using a number of different approaches. The number of new defects was determined using the Wigner-Seitz (WS) method as implemented in OVITO [36], while dislocations were identified using OVITO's DXA analysis [37]. The average radius of cascades in the pristine material was calculated as follows: During the simulations, local energetic regions were identified on-the-fly, by periodically outputting atoms for which the atom and its neighbors had an average kinetic energy higher than a given threshold, which in this case was set to the melting point as predicted by the interatomic potential. The cascade center was defined to be the center of mass of this "liquid" region at its largest, weighted by the kinetic energy of the atoms. The volume of the cascade region was calculated by computing a surface mesh for the disordered atoms using OVITO. The cascade radius was then calculated under the assumption of a spherical cascade region.

4. Results

4.1. Defect numbers

Fig. 2 shows the number of new Frenkel pairs formed as a function of the size of the pre-existing void, plotted on a logarithmic scale. Lines are given by Eq. (2), fitted to the data points. The slope of these lines is given by the parameter a, and displays a clear energy dependence, with higher energies having a steeper slope. Table 3 gives the average number of Frenkel pairs produced in pris-

Table 2
The pre-existing void sizes used in this study, in terms of numbers of vacancies N_{Vac} and the number of runs for each different cascade energy.

N_{vac}	1 keV	5 keV	10 keV	20 keV	30 keV	50 keV	70 keV	100 keV
0	200	200	200	200	100	100	100	100
2	200	200	200	200	100			
4	200	200	200	200	100			
8		200	200	200	100			
10	200	200	200	100	100			
27	200	200	200	200	100	200	200	
59	200	200	200	200	100	200	100	100
259	200	200	200	200	100	100	100	100
893	200	200	200	200	100	100	100	100
2085		200	200	200	100	100	100	100

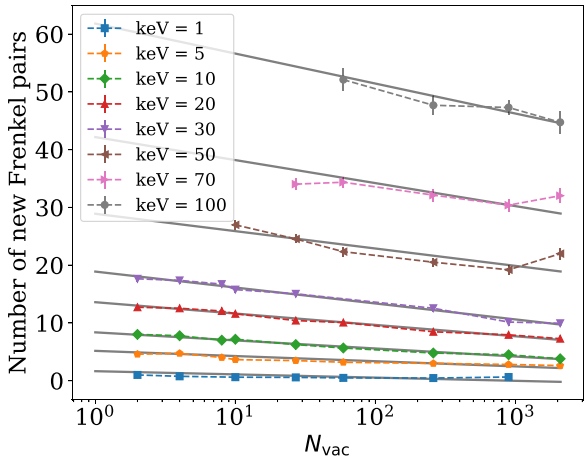

Fig. 2. Number of new Frenkel pairs (N_{new}) from cascades overlapping with the pre-existing void, as a function of the size of the void expressed in terms of the number of vacancies it contained (N_{vac}). Lines are given by Eq. (2) fitted to the data points. The uncertainty of the data points is given by the standard error.

Table 3
Average number of Frenkel pairs in pristine material for each cascade energy, with the uncertainty given by the standard error.

E_{PKA}	1 keV	5 keV	10 keV	20 keV
	30 keV	50 keV	70 keV	100 keV
N_0	1.64 ± 0.06	5.2 ± 0.12	8.4 ± 0.19	13.6 ± 0.3
	18.9 ± 0.5	28.9 ± 0.7	42.2 ± 1.2	61.8 ± 1.8

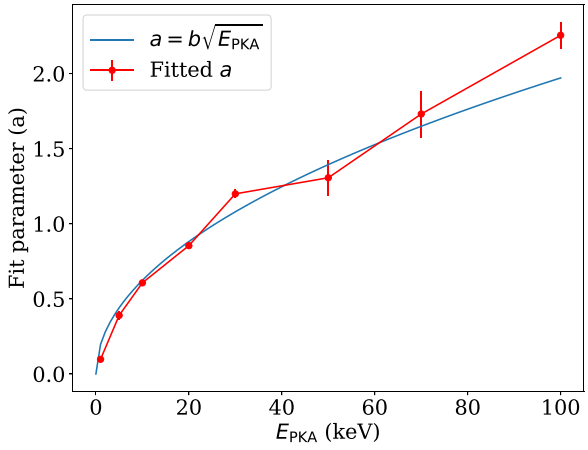

Fig. 3. Fitting parameter a as a function of cascade energy.The uncertainty is given as the standard deviation.

tine systems (N_0) for each E_{PKA} respectively. These values were also used in the fitting of Eq. (2), although they have been excluded from the plot in Fig. 2 due to the logarithmic scale.

In Fig. 3, we plot the parameter a from Eq. (2), as a function of the cascade energy. The energy dependence of a is well described by a square root function:

$$a = b\sqrt{E_{PKA}} \tag{3}$$

The parameter b was determined by fitting Eq. (3) to the obtained values for a, and was found to be $b = 0.1970 \pm 0.0079$. The uncertainty of this parameter is the standard deviation coming from the fitting of Eq. (2).

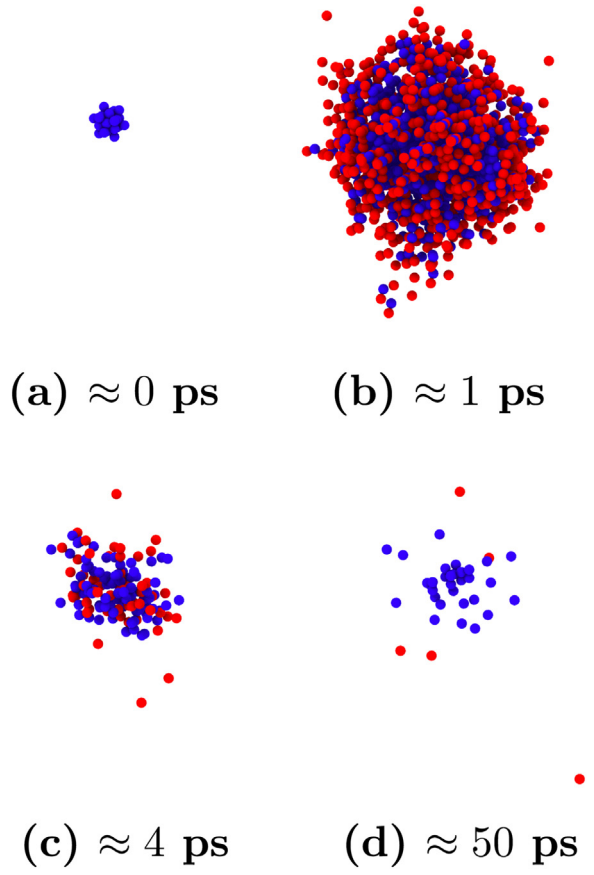

Fig. 4. Example cascade with PKA energy of 20 keV and an initial void containing 27 vacancies. Blue spheres represent vacancies and red spheres represent interstitials as identified by WS-analysis.

4.2. Defect morphology

Generally, we find that the pre-existing void has a significant impact on the likelihood of dislocation line formation, as well as on the types of dislocations that are formed as a direct result of the cascade. If fully enveloped by the cascade, the pre-existing void is essentially destroyed, and the recrystallization of the heat spike determines the surviving defect structure. Fig. 4 shows an example case where the pre-existing defect is fully enveloped by a cascade. The situation is similar also when the pre-existing defect is situated nearer to the border but still within the cascade region. In either case, the pre-existing defect cannot be identified after the cascade. In contrast, Fig. 5 shows a case of a cascade that only partially overlaps with a larger void. In this case the vacancies encompassed within the cascade region collapse to form a $\langle 1\,0\,0 \rangle$ dislocation loop, while the rest of the void remains intact. For the high energy PKAs and larger pre-existing voids, this kind of behaviour was observed frequently.

We observed the formation of vacancy-type dislocation loops of different sizes, and with both $\langle 1\,0\,0 \rangle$ and $1/2\langle 1\,1\,1 \rangle$ Burgers vectors. Vacancies drawn from the pre-existing void played a key role in the formation of vacancy-type loops, as in the example illustrated in Fig. 5. On the other hand, the interstitial-type loops found in this study were mainly small, and of $1/2\langle 1\,1\,1 \rangle$ type. Occasionally, dislocation lines terminating in the void were also observed.

We classify the final damage configurations into four categories: categories (a) and (b) include well formed dislocation loops with Burgers vector $\langle 1\,0\,0 \rangle$ and $1/2\langle 1\,1\,1 \rangle$, respectively; category (c) contains dislocation lines that either do not close to form a loop (i.e. they terminate in the void structure), or form branching disloca-

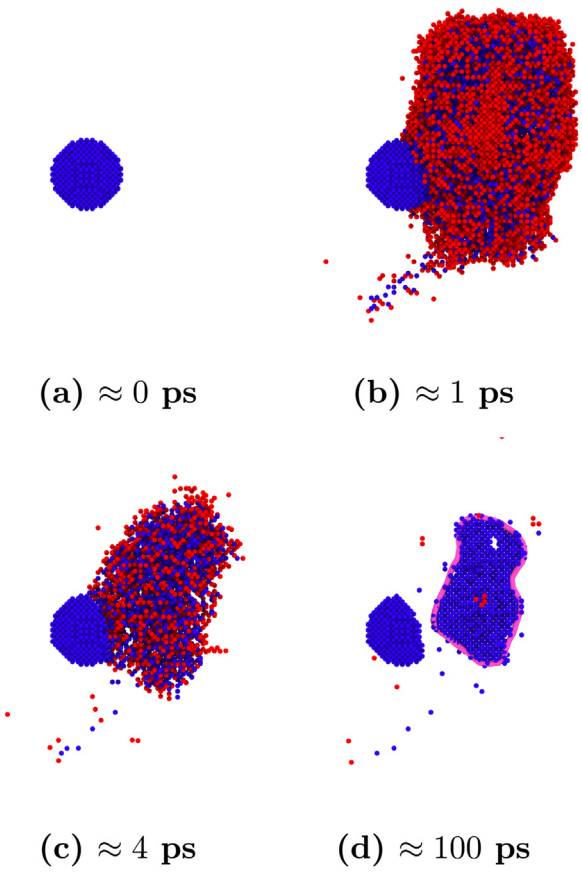

Fig. 5. Example cascade with PKA energy of 100 keV and an initial void containing 2085 vacancies. Blue spheres represent vacancies and red spheres represent interstitials as identified by WS-analysis. Magenta line represents a ⟨1 0 0⟩ dislocation loop as identified by the DXA-analysis.

tions, which we collectively label as *open*; and finally category (d) includes damage with no identifiable dislocations, labelled *none*. The debris from a given cascade may belong to multiple categories simultaneously.

In Fig. 6, we plot the fractions of cascades that produce defects belonging to these different categories. It is clear that the probability of finding any dislocation structure grows with increasing cascade energy (as the fraction of "none" decreases, see panel (d) in Fig. 6). Conversely, we find that the production of ⟨1 0 0⟩ dislocations (a) and "open" dislocation structures (c) shows a stronger dependence on the size of the initial void than on the PKA energy, and are observed for pre-existing void sizes above $N_{\text{vac}} = 27$ vacancies. $1/2\langle 1\,1\,1\rangle$ dislocation formation, on the other hand, is more dependent on the cascade energy than on the size of the pre-existing void.

5. Discussion

In the case of small pre-existing vacancy clusters, the overlapping cascade fully envelops the defect. Hence, in this range, the larger the defect is, the more it affects the cascade evolution. This is seen clearly for the 100 keV PKAs as the void size increases. For the lower PKA energies and larger voids studied here, however, the cascade radius is smaller than or comparable to the radius of the void. In these cases, the cascade cannot fully envelop the void, hence increasing the void size mainly adds to the void outside the cascade region. For the largest voids and smallest cascades, the void radius is up to four times larger than the cascade radius, thus the void appears much like a surface from the point of view of the cascade evolution, and the size of the void becomes somewhat irrelevant. This explains why the effect of increasing void size in the range studied here is negligible for 1 keV cascades, and grows as the PKA energy increases. Table 4 lists the ratios between the different cascade radii and pre-existing void radii

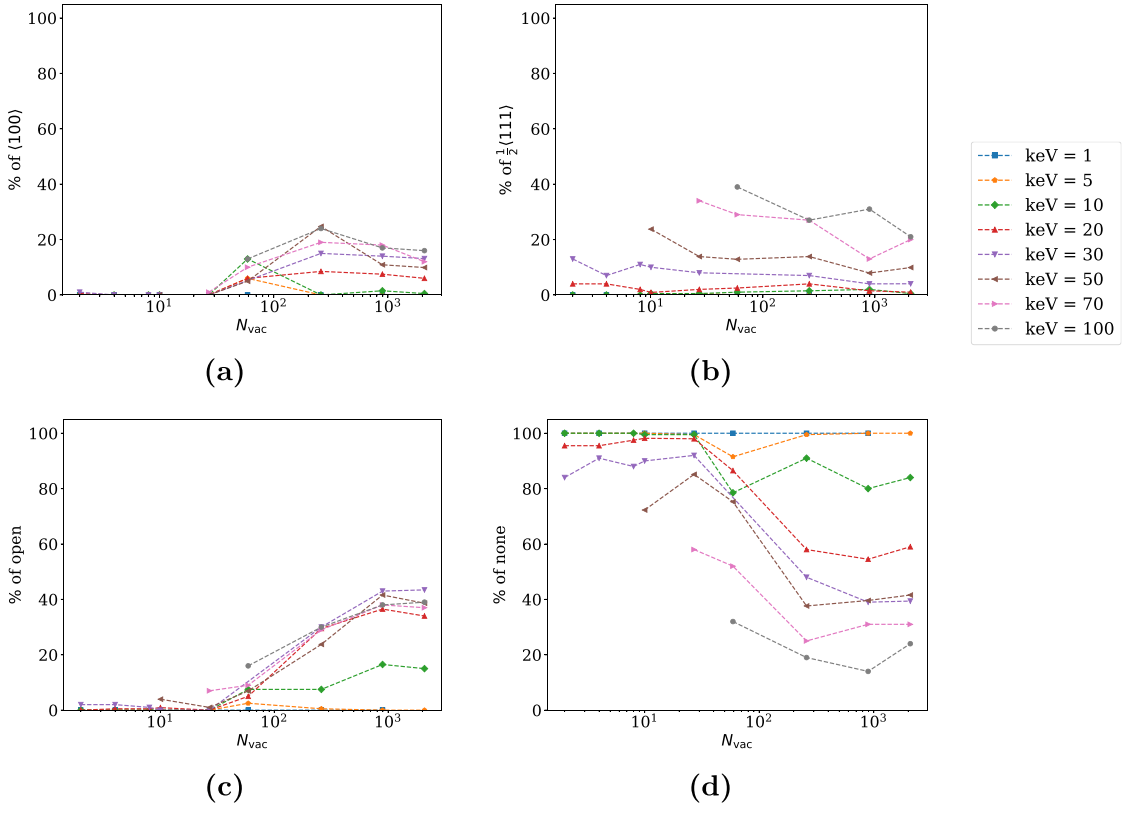

Fig. 6. Percentage of dislocation structures identified by DXA analysis, as a function of the size of the pre-existing void in terms of the vacancy content N_{Vac}.

Table 4
The ratios (r_{casc}/r_{void}) between the cascade and void radii, for the larger void sizes studied here. The second column gives the average cascade radius r_{casc} calculated from cascade simulations in pristine crystal, with the corresponding PKA energies listed in the first column. The void radii r_{void} are given above the last 5 columns.

		r_{void} (Å)				
E_{PKA} (keV)	r_{casc} (Å)	5	6	10	15	20
1	4.99	0.9996	0.833	0.4998	0.3332	0.2499
5	15.5	3.1012	2.5843	1.5506	1.0337	0.7753
10	19.66	3.932	3.2767	1.966	1.3107	0.983
20	25.91	5.1828	4.319	2.5914	1.7276	1.2957
30	29.67	5.9341	4.9451	2.967	1.978	1.4835
50	35.31	7.0615	5.8845	3.5307	2.3538	1.7654
70	39.28	7.8552	6.546	3.9276	2.6184	1.9638
100	44.22	8.844	7.37	4.422	2.948	2.211

for the range of void sizes that become comparable to the cascade size. For the 100 keV cascades, all voids are smaller than the cascade radius. One can expect that, if the void size further increases, the impact on the new defect numbers eventually saturates. This regime would be beyond the range of validity of the model presented here.

The data for lower PKA energies follow closely the square root function in Eq. (3) used to describe the energy dependence of the parameter a. In the higher energy region, for PKA energies above 10 keV, a linear model would fit the data more closely. However, this would give incorrect results for the lower energy recoils. The low energy limit of the recoil energy spectrum is important for e.g. neutron and light ion irradiation, where low energy recoils are frequent. In addition, for higher PKA energies, beyond the data obtained in this study, the value of a can be expected to saturate, as sub-cascade splitting [38] causes the cascade to split into pockets of disconnected lower energy cascade regions, only one of which may overlap with the void. Hence, a linear model would seriously over-predict the value of a in the high energy limit. With these considerations, we conclude that the square root function captures adequately both the high energy and low energy limits. For very high energy PKAs, the void density would become important, through the probability of the separate cascade pockets overlapping with several voids. The spatial extent and distribution of cascade pockets can be modelled e.g. using BCA methods Backer et al. [38], but this is beyond the scope of the current work.

6. Conclusions

In this work, a large number of cascade simulations were performed with different PKA energies, overlapping with pre-existing voids of different sizes. The production of additional Frenkel pairs due to the overlapping cascades shows a logarithmic dependence on the pre-existing void size for all PKA energies studied here. We find that the energy dependence of the logarithmic functions can be well described using a square root function. The model presented and parametrized here can be used to adjust KMC and rate theory simulations of radiation damage accumulation.

Furthermore, we find that both the cascade energy and the size of the pre-existing void impacts the frequency and morphology of dislocations produced by the overlapping cascades. Differences between dislocation loops with different Burgers vectors were observed, with $\langle 1\,0\,0\rangle$ dislocations showing a stronger dependence on the size of the pre-existing void, while the frequency of formation of $1/2\langle 1\,1\,1\rangle$ loops depended mainly on the PKA energy. Larger pre-existing voids were found to induce the formation of $\langle 1\,0\,0\rangle$ dislocation loops even for relatively low PKA energies.

For explicit morphology of the damage, the final configurations from this work are available in the IAEA CascadesDB database (https://cascadesdb.iaea.org/).

Data availability

Recoil energy dependence of primary radiation damage in tungsten from cascade overlap with voids (Mendeley Data).

Declaration of Competing Interest

The authors declare that they have no known competing financial interests or personal relationships that could have appeared to influence the work reported in this paper.

CRediT authorship contribution statement

A. Fellman: Methodology, Data curation, Investigation, Visualization, Writing – original draft. **A.E. Sand:** Methodology, Conceptualization, Funding acquisition, Resources, Supervision, Writing – review & editing.

Acknowledgements

This work has been carried out within the framework of the EUROfusion Consortium, funded by the European Union via the Euratom Research and Training Programme (Grant agreement no. 101052200 — EUROfusion). Views and opinions expressed are however those of the author(s) only and do not necessarily reflect those of the European Union or the European Commission. Neither the European Union nor the European Commission can be held responsible for them. We acknowledge the Finnish Grid and Cloud Infrastructure (persistent identifier urn:nbn:fi:research-infras-2016072533) and CSC – IT Center for Science, Finland, for computational resources.

References

[1] R. Pitts, S. Carpentier, F. Escourbiac, T. Hirai, V. Komarov, S. Lisgo, A. Kukushkin, A. Loarte, M. Merola, A. Sashala Naik, R. Mitteau, M. Sugihara, B. Bazylev, P. Stangeby, A full tungsten divertor for iter: physics issues and design status, J. Nucl. Mater. 438 (2013) S48–S56, doi:10.1016/j.jnucmat.2013.01.008. Proceedings of the 20th International Conference on Plasma-Surface Interactions in Controlled Fusion Devices.

[2] V. Philipps, Tungsten as material for plasma-facing components in fusion devices, J. Nucl. Mater. 415 (1, Supplement) (2011) S2–S9, doi:10.1016/j.jnucmat.2011.01.110. Proceedings of the 19th International Conference on Plasma-Surface Interactions in Controlled Fusion.

[3] M. Rieth, S. Dudarev, S.G. de Vicente, J. Aktaa, T. Ahlgren, S. Antusch, D. Armstrong, M. Balden, N. Baluc, M.-F. Barthe, W. Basuki, M. Battabyal, C. Becquart, D. Blagoeva, H. Boldyryeva, J. Brinkmann, M. Celino, L. Ciupinski, J. Correia, A.D. Backer, C. Domain, E. Gaganidze, C. García-Rosales, J. Gibson, M. Gilbert, S. Giusepponi, B. Gludovatz, H. Greuner, K. Heinola, T. Höschen, A. Hoffmann, N. Holstein, F. Koch, W. Krauss, H. Li, S. Lindig, J. Linke, C. Linsmeier, P. López-Ruiz, H. Maier, J. Matejicek, T. Mishra, M. Muhammed, A. Muñoz, M. Muzyk, K. Nordlund, D. Nguyen-Manh, J. Opschoor, N. Ordás, T. Palacios, G. Pintsuk, R. Pippan, J. Reiser, J. Riesch, S. Roberts, L. Romaner, M. Rosiński, M. Sanchez, W. Schulmeyer, H. Traxler, A. Ureña, J. van der Laan, L. Veleva, S. Wahlberg, M. Walter, T. Weber, T. Weitkamp, S. Wurster, M. Yar, J. You, A. Zivelonghi, Recent progress in research on tungsten materials for nuclear fusion applications in europe, J. Nucl. Mater. 432 (1) (2013) 482–500, doi:10.1016/j.jnucmat.2012.08.018. http://www.sciencedirect.com/science/article/pii/S0022311512004278.

[4] H. Bolt, V. Barabash, G. Federici, J. Linke, A. Loarte, J. Roth, K. Sato, Plasma facing and high heat flux materials – needs for iter and beyond, J. Nucl. Mater. 307–311 (2002) 43–52, doi:10.1016/S0022-3115(02)01175-3. http://www.sciencedirect.com/science/article/pii/S0022311502011753.

[5] J. Marian, C.S. Becquart, C. Domain, S.L. Dudarev, M.R. Gilbert, R.J. Kurtz, D.R. Mason, K. Nordlund, A.E. Sand, L.L. Snead, et al., Recent advances in modeling and simulation of the exposure and response of tungsten to fusion energy conditions, Nucl. Fusion 57 (9) (2017) 092008.

[6] K. Nordlund, S.J. Zinkle, A.E. Sand, F. Granberg, R.S. Averback, R. Stoller, T. Suzudo, L. Malerba, F. Banhart, W.J. Weber, F. Willaime, S. Dudarev, D. Simeone, Primary radiation damage: a review of current understanding and models, J. Nucl. Mater. 512 (2018) 450–479.

[7] I. Robertson, M. Kirk, W.E. King, Formation of dislocation loops in iron by self-ion irradiations at 40k, Scr. Metall. 18 (4) (1984) 317–320, doi:10.1016/0036-9748(84)90444-7. http://www.sciencedirect.com/science/article/pii/0036974884904447.
[8] F. Gao, D. Bacon, A. Calder, P. Flewitt, T. Lewis, Computer simulation study of cascade overlap effects in α-iron, J. Nucl. Mater. 230 (1) (1996) 47–56, doi:10.1016/0022-3115(96)00020-7. http://www.sciencedirect.com/science/article/pii/0022311596000207.
[9] M.W. Ullah, D.S. Aidhy, Y. Zhang, W.J. Weber, Damage accumulation in ion-irradiated ni-based concentrated solid-solution alloys, Acta Mater. 109 (2016) 17–22.
[10] F. Granberg, J. Byggmästar, A.E. Sand, K. Nordlund, Cascade debris overlap mechanism of ⟨100⟩ dislocation loop formation in Fe and FeCr, EPL (Europhys. Lett.) 119 (5) (2017) 56003.
[11] K. Lai, K. Li, H. Wen, Q. Guo, B. Wang, Y. Zheng, Synergistic effects of applied strain and cascade overlap on irradiation damage in bcc iron, J. Nucl. Mater. 542 (2020) 152422.
[12] Y. Wang, W. Lai, J. Li, An incremental model for defect production upon cascade overlapping, Chin. Phys. Lett. 37 (1) (2020) 016103.
[13] F. Granberg, K. Nordlund, M.W. Ullah, K. Jin, C. Lu, H. Bei, L.M. Wang, F. Djurabekova, W.J. Weber, Y. Zhang, Mechanism of radiation damage reduction in equiatomic multicomponent single phase alloys, Phys. Rev. Lett. 116 (2016) 135504.
[14] E. Levo, F. Granberg, C. Fridlund, K. Nordlund, F. Djurabekova, Radiation damage buildup and dislocation evolution in equiatomic multicomponent alloys, J. Nucl. Mater. 490 (2017) 323.
[15] P.K. Nandi, J. Eapen, Cascade overlap in HCP zirconium: defect accumulation and microstructure evolution with radiation using molecular dynamics simulations, in: MRS Proceedings, vol. 1514, 2013, pp. 37–42, doi:10.1557/opl.2013.122.
[16] C. Dai, F. Long, P. Saidi, L.K. Béland, Z. Yao, M.R. Daymond, Primary damage production in the presence of extended defects and growth of vacancy-type dislocation loops in HCP zirconium, Phys. Rev. Mater. 3 (2019) 043602.
[17] A. Diver, O. Dicks, A.M. Elena, I.T. Todorov, K. Trachenko, Evolution of amorphous structure under irradiation: zircon case study, J. Phys. 32 (41) (2020) 415703.
[18] S. Zhang, B.W. Wang, L.M. Zhang, N. Liu, T.S. Wang, B.H. Duan, X.G. Xu, Defect agglomeration induces a reduction in radiation damage resistance of In-rich $In_xGa_{1-x}N$, J. Phys. D 54 (24) (2021) 245104.
[19] F. Granberg, J. Byggmästar, K. Nordlund, Defect accumulation and evolution during prolonged irradiation of Fe and FeCr alloys, J. Nucl. Mater. 528 (2020) 151843, doi:10.1016/j.jnucmat.2019.151843. https://www.sciencedirect.com/science/article/pii/S0022311519305719.
[20] F. Granberg, J. Byggmästar, K. Nordlund, Molecular dynamics simulations of high-dose damage production and defect evolution in tungsten, J. Nucl. Mater. 556 (2021) 153158, doi:10.1016/j.jnucmat.2021.153158. https://www.sciencedirect.com/science/article/pii/S0022311521003810.
[21] K. Nordlund, R.S. Averback, Point defect movement and annealing in collision cascades, Phys. Rev. B 56 (5) (1997) 2421–2431.
[22] D. Terentyev, K. Vörtler, C. Björkas, K. Nordlund, L. Malerba, Primary radiation damage in bcc Fe and Fe-Cr crystals containing dislocation loops, J. Nucl. Mater. 417 (2011) 1063–1066.
[23] J. Byggmästar, F. Granberg, A.E. Sand, A. Pirttikoski, R. Alexander, M.-C. Marinica, K. Nordlund, Collision cascades overlapping with self-interstitial defect clusters in Fe and W, J. Phys. 31 (24) (2019) 245402, doi:10.1088/1361-648x/ab0682.
[24] A.E. Sand, S.L. Dudarev, K. Nordlund, High energy collision cascades in tungsten: dislocation loops structure and clustering scaling laws, EPL 103 (2013) 46003.
[25] A. Sand, K. Nordlund, S. Dudarev, Radiation damage production in massive cascades initiated by fusion neutrons in tungsten, J. Nucl. Mater. 455 (1–3) (2014) 207–211.
[26] M. Gilbert, J. Marian, J.-C. Sublet, Energy spectra of primary knock-on atoms under neutron irradiation, J. Nucl. Mater. 467 (Part 1) (2015) 121–134, doi:10.1016/j.jnucmat.2015.09.023. http://www.sciencedirect.com/science/article/pii/S0022311515302129.
[27] A. Sand, J. Byggmästar, A. Zitting, K. Nordlund, Defect structures and statistics in overlapping cascade damage in fusion-relevant bcc metals, J. Nucl. Mater. 511 (2018) 64–74.
[28] A. Hasegawa, M. Fukuda, T. Tanno, S. Nogami, Neutron irradiation behavior of tungsten, Mater. Trans. 54 (4) (2013) 466–471, doi:10.2320/matertrans.MG201208.
[29] A. Fellman, A.E. Sand, J. Byggmästar, K. Nordlund, Radiation damage in tungsten from cascade overlap with voids and vacancy clusters, J. Phys. 31 (40) (2019) 405402, doi:10.1088/1361-648x/ab2ea4.
[30] H.J. Berendsen, J.v. Postma, W.F. van Gunsteren, A. DiNola, J. Haak, Molecular dynamics with coupling to an external bath, J. Chem. Phys. 81 (8) (1984) 3684–3690.
[31] K. Nordlund, 2010, PARCAS computer code. The main principles of the molecular dynamics algorithms are presented in [39,40]. The adaptive time step and electronic stopping algorithms are the same as in [41].
[32] G.J. Ackland, R. Thetford, An improved n-body semi-empirical model for body-centred cubic transition metals, Philos. Mag. A 56 (1) (1987) 15–30, doi:10.1080/01418618708204464.
[33] Y. Zhong, K. Nordlund, M. Ghaly, R.S. Averback, Defect production in tungsten: a comparison between field-ion microscopy and molecular-dynamics simulations, Phys. Rev. B 58 (1998) 2361–2364, doi:10.1103/PhysRevB.58.2361.
[34] A. Sand, J. Dequeker, C. Becquart, C. Domain, K. Nordlund, Non-equilibrium properties of interatomic potentials in cascade simulations in tungsten, J. Nucl. Mater. 470 (2016) 119–127.
[35] J. Ziegler, J. Biersack, U. Littmark, The Stopping and Range of Ions in Matter, Pergamon, New York, 1985.
[36] A. Stukowski, Visualization and analysis of atomistic simulation data with ovito–the open visualization tool, Model. Simul. Mater. Sci. Eng. 18 (1) (2010) 015012. http://stacks.iop.org/0965-0393/18/i=1/a=015012.
[37] A. Stukowski, K. Albe, Extracting dislocations and non-dislocation crystal defects from atomistic simulation data, Model. Simul. Mater. Sci. Eng. 18 (8) (2010) 085001. http://stacks.iop.org/0965-0393/18/i=8/a=085001.
[38] A.D. Backer, A.E. Sand, K. Nordlund, L. Luneville, D. Simeone, S.L. Dudarev, Subcascade formation and defect cluster size scaling in high-energy collision events in metals, EPL Europhys. Lett. 115 (2) (2016) 26001.